

torial humid belt in the Late Triassic was comparable to today's (Fig. 3), a conclusion that contrasts with some previous suggestions of a much more restricted or even dry equatorial belt in the Triassic (33, 34). Poleward motion can explain the generally drier northward and up-section facies pattern in the Mesozoic rift basins of eastern North America (32, 35) as this part of Pangea drifted out of the equatorial humid belt. At the same time, the up-section progression to more humid facies in the Fleming Fjord Formation (36, 37) and the overlying plant-bearing Kap Stewart Formation of latest Triassic and earliest Jurassic age (38) in the Jameson Land basin would reflect the drift of this area into the temperate humid belt.

We conclude that the congruence of the corrected paleomagnetic data from sedimentary rocks and independent data from igneous rocks ranging over thousands of kilometers and tens of millions of years indicates that a GAD field similar to that of the past 5 My was operative at least 200 Ma in the Late Triassic and earliest Jurassic. In particular, we see no evidence for a major octupole contribution in either the shapes of the distributions of directions in the sedimentary units or in the geographic distribution of site paleolatitudes. As indicated by other recent studies (17, 39–41), there is thus little empirical basis to invoke persistent departures from the GAD field, especially zonal octupole contributions, to address tectonic problems (4, 42, 43). Instead, our results suggest that inclination error in sedimentary rocks may be more prevalent than has been supposed, perhaps especially in cases where the magnetizations that have been isolated are most likely to represent a depositional remanence carried by hematite. The success of the E/I method (17) to determine the degree of flattening and to correct any bias in inclinations from the distribution of directions should provide motivation for more intensive sampling of sedimentary rock units and for making detailed data more accessible.

#### References and Notes

- J. Hospers, *Nature* **173**, 1183 (1954).
- C. L. Johnson, C. G. Constable, *Geophys. J. Int.* **131**, 643 (1997).
- R. T. Merrill, P. L. McFadden, *Phys. Earth Planet. Inter.* **139**, 171 (2003).
- R. Van der Voo, T. H. Torsvik, *Earth Planet. Sci. Lett.* **187**, 71 (2001).
- J. Si, R. Van der Voo, *Terra Nova* **13**, 471 (2001).
- M. Westphal, *Earth Planet. Sci. Lett.* **117**, 15 (1993).
- R. F. King, *Mon. Not. R. Astron. Soc. Geophys. Suppl.* **7**, 115 (1955).
- L. Tauxe, D. V. Kent, *Geophys. J. R. Astron. Soc.* **77**, 543 (1984).
- P. Olsen, D. V. Kent, B. Cornet, W. K. Witte, R. W. Schlische, *Geol. Soc. Am. Bull.* **108**, 40 (1996).
- D. V. Kent, P. E. Olsen, W. K. Witte, *J. Geophys. Res.* **100**, 14 (1995).
- D. V. Kent, P. E. Olsen, *J. Geophys. Res.* **104**, 12 (1999).
- D. V. Kent, P. E. Olsen, *Geol. Soc. Am. Bull.* **109**, 366 (1997).
- D. V. Kent, P. E. Olsen, *Earth Planet. Sci. Lett.* **179**, 311 (2000).
- D. V. Kent, L. B. Clemmensen, *Bull. Geol. Soc. Den.* **42**, 121 (1996).
- W. R. Roest, S. P. Srivastava, *Geology* **17**, 1000 (1989).
- E. C. Bullard, J. E. Everett, A. G. Smith, *Philos. Trans. R. Soc. London Ser. A* **258**, 41 (1965).
- L. Tauxe, D. V. Kent, *Geophys. Monogr. Am. Geophys. Union* **145**, 101 (2004).
- C. G. Constable, R. L. Parker, *J. Geophys. Res.* **93**, 11 (1988).
- J. C. Briden, B. A. Daniels, *J. Geol. Soc. London* **156**, 317 (1999).
- A. Marzoli *et al.*, *Science* **284**, 616 (1999).
- M. Prevot, M. McWilliams, *Geology* **17**, 1007 (1989).
- J. P. Hodych, A. Hayatsu, *Can. J. Earth Sci.* **25**, 1972 (1988).
- J. Pohl, H. Soffel, *Zeitschrift fur Geophysik* **37**, 857 (1971).
- W. A. Robertson, *Can. J. Earth Sci.* **4**, 641 (1967).
- A. Larochele, K. L. Currie, *J. Geophys. Res.* **72**, 4163 (1967).
- J. P. Hodych, G. R. Dunning, *Geology* **20**, 51 (1992).
- S. P. Kelley, J. G. Spray, *Meteorit. Planet. Sci.* **32**, 629 (1997).
- N. D. Opdyke, *J. Geophys. Res.* **66**, 1941 (1961).
- W. K. Witte, D. V. Kent, *J. Geophys. Res.* **96**, 19 (1991).
- J. L. Roy, *Earth Planet. Sci. Lett.* **14**, 103 (1972).
- E. I. Robbins, G. P. Wilkes, D. A. Textoris, in *Triassic–Jurassic Rifting: North America and Africa*, W. Manspeizer, Ed. (Elsevier, Amsterdam, 1988), pp. 649–682.
- J. F. Hubert, K. A. Mertz, *Geology* **8**, 516 (1980).
- K. M. Wilson, D. Pollard, W. W. Hay, S. L. Thompson, C. N. Wold, *Geol. Soc. Am. Spec. Pap.* **288**, 91 (1994).
- J. T. Parrish, *Journal of Geology* **101**, 215 (1993).
- J. P. Smoot, *Palaeogeogr. Palaeoclimatol. Palaeoecol.* **84**, 369 (1991).
- L. B. Clemmensen, D. V. Kent, F. A. Jenkins Jr., *Palaeogeogr. Palaeoclimatol. Palaeoecol.* **140**, 135 (1998).
- L. B. Clemmensen, *Geol. Surv. Greenland Bull.* **136**, 5 (1980).
- J. C. McElwain, D. J. Beerling, F. I. Woodward, *Science* **285**, 1386 (1999).
- G. Muttoni *et al.*, *Earth Planet. Sci. Lett.* **215**, 379 (2003).
- S. Gilder *et al.*, *Earth Planet. Sci. Lett.* **206**, 587 (2003).
- W. Krijgsman, L. Tauxe, *Earth Planet. Sci. Lett.* **222**, 685 (2004).
- T. H. Torsvik, R. Van der Voo, *Geophys. J. Int.* **151**, 771 (2002).
- P. Rochette, D. Vandamme, *Ann. Geofis.* **44**, 649 (2001).
- NASA, Visible Earth, available at <http://visibleearth.nasa.gov/>.
- T. J. Crowley, G. R. North, *Oxford Monogr. Geol. Geophys.* **18** (1991).
- We thank P. Olsen for many discussions of the Triassic–Jurassic world and the reviewers for insightful comments. Supported by National Science Foundation grant nos. EAR–0310240 (D.V.K.) and EAR–0003395 (L.T.). This is LDEO contribution #6700.

#### Supporting Online Material

[www.sciencemag.org/cgi/content/full/307/5707/240/DC1](http://www.sciencemag.org/cgi/content/full/307/5707/240/DC1)

Fig. S1

References and Notes

29 September 2004; accepted 9 December 2004  
10.1126/science.1105826

## An Astronomical 2175 Å Feature in Interplanetary Dust Particles

John Bradley,<sup>1\*</sup> Zu Rong Dai,<sup>1</sup> Rolf Erni,<sup>2</sup> Nigel Browning,<sup>2,3</sup> Giles Graham,<sup>1</sup> Peter Weber,<sup>1</sup> Julie Smith,<sup>1</sup> Ian Hutcheon,<sup>1</sup> Hope Ishii,<sup>1</sup> Sasa Bajt,<sup>1</sup> Christine Floss,<sup>4</sup> Frank Stadermann,<sup>4</sup> Scott Sandford<sup>5</sup>

The 2175 angstrom extinction feature is the strongest (visible-ultraviolet) spectral signature of dust in the interstellar medium. Forty years after its discovery, the origin of the feature and the nature of the carrier(s) remain controversial. Using a transmission electron microscope, we detected a 5.7–electron volt (2175 angstrom) feature in interstellar grains embedded within interplanetary dust particles (IDPs). The carriers are organic carbon and amorphous silicates that are abundant in IDPs and in the interstellar medium. These multiple carriers may explain the enigmatic invariant central wavelength and variable bandwidth of the astronomical 2175 angstrom feature.

Much of what is known about grains in space comes from spectral features observed in emission, polarization, and absorption (1–7). The 2175 Å peak is by far the strongest feature observed in the ultraviolet (UV)–

visible wavelength range along most lines of sight for which it can be measured (Fig. 1, A and B) (4–7). The feature is enigmatic: Its central wavelength is almost invariant, but its bandwidth varies from one line of sight to another, suggesting multiple carriers or a single carrier with variable properties. From interstellar abundances of the elements and typical UV transition strengths, the carrier is either oxygen-rich (e.g., oxides or silicates) or carbon-rich (e.g., graphite or organic compounds) (1–4, 8). We searched UV spectra of chondritic IDPs for an extinction feature near the ~2175 Å interstellar feature (Fig. 1). Materials similar to the two most abundant grain types seen in the

<sup>1</sup>Institute of Geophysics and Planetary Physics, Lawrence Livermore National Laboratory, Livermore, CA 94550, USA. <sup>2</sup>Department of Chemical Engineering, University of California at Davis, CA 95616, USA. <sup>3</sup>National Center for Electron Microscopy, Lawrence Berkeley National Laboratory, Berkeley, CA 94720, USA. <sup>4</sup>Laboratory for Space Sciences, Washington University, St. Louis, MO 63130, USA. <sup>5</sup>Astrophysics Branch, NASA–Ames Research Center, Moffett Field, CA 94035, USA.

\*To whom correspondence should be addressed.  
E-mail: jbradley@igpp.uclln.org

interstellar medium (ISM), amorphous silicates and carbonaceous matter, are found in IDPs (Fig. 2) (9). The amorphous silicates are glass with embedded metal and sulfides (GEMS), some with nonsolar O isotopic compositions (10–13). The carbonaceous matter is a mixture of inorganic and organic carbon, and some of the organic materials exhibit nonsolar D/H,  $^{15}\text{N}/^{14}\text{N}$ , and  $^{13}\text{C}/^{12}\text{C}$  ratios comparable in magnitude to those observed in interstellar molecular clouds (13–15). The nonsolar isotopic signatures establish that these GEMS and carbonaceous subgrains are of interstellar origin.

We used a new-generation transmission electron microscope (TEM) equipped with a monochromator and high-resolution electron energy-loss spectrometer to measure UV spectral properties of portions of IDPs and standards (16, 17). The 0- to  $\sim 100$ -eV region of an energy-loss spectrum, known as the valence electron energy-loss spectroscopy (VEELS) region (17), includes the 2175 Å (5.7 eV) UV spectral feature. We used VEELS because the submicrometer dimensions of the subgrains preclude measurement by conventional photoabsorption spectroscopy (PAS). The VEELS data were acquired under conditions in which the positions of VEELS and PAS features are comparable, but PAS typically has  $\sim 10$  times better wavelength/energy resolution (18). A synchrotron light source was used to measure infrared (IR) spectral properties (17), and two NanoSIMS (secondary ion mass spectrometry) microprobes were used to measure the isotopic compositions of grains within the same IDPs (17).

A VEELS spectrum from the mineral talc ( $\text{Mg}_3\text{Si}_4\text{O}_{10}[\text{OH}]_2$ ) shows a peak position and bandwidth that match the photoabsorption feature of hydroxylated amorphous  $\text{Mg}_2\text{SiO}_4$  (Fig. 1, C and D) (8), as well as the astronomical UV feature (Fig. 1, A, B, and D). VEELS spectra from carbonaceous grains in three IDPs exhibit a 5.7-eV feature with average bandwidth (full width at half maximum, FWHM) of 2.6 eV ( $2.2 \mu\text{m}^{-1}$ ) (Fig. 3, A to C). With increasing O/C ratio, the strength of the 5.7-eV feature increases and the peak of the volume plasmon (the broad peak between 10 and 28 eV) decreases in energy. Energy-loss C and O core scattering edges from the most O-rich regions exhibit a fine structure consistent with carbonyl (or hydroxyl) functional groups (19), and IR spectra there exhibit prominent C-H stretch and C=O features at  $\sim 3.4 \mu\text{m}$  and  $\sim 5.9 \mu\text{m}$ , respectively (Fig. 4). Although the signal-to-noise ratio is marginal, because the IR spectrum was acquired from a  $\sim 9\text{-}\mu\text{m}^2$  area  $\sim 0.1 \mu\text{m}$  thick, the overall structure of the C-H stretch feature between 2850 and  $3100 \text{ cm}^{-1}$  in L2036 G16 (and in other IDPs) is consistent

with aliphatic groups bound to other molecules like polycyclic aromatic hydrocarbons (PAHs) (19–21). 1-Pyrene carboxaldehyde ( $\text{C}_{17}\text{H}_{10}\text{O}$ ) exhibits the  $\sim 5.7$ -eV feature but pyrene ( $\text{C}_{16}\text{H}_{10}$ ), with no carbonyl group, produces a feature that is shifted to higher energy ( $\sim 6.1$  eV) (Fig. 3, D and E). GEMS produce a 5.7-eV feature with an average bandwidth (FWHM) of 2.9 eV ( $2.5 \mu\text{m}^{-1}$ ), and the feature strength correlates with hydroxyl ( $\text{OH}^-$ ) content (Fig. 3, F to J). Thus, both organic compounds and amorphous silicates in IDPs may be carriers of a 5.7-eV feature.

The central wavelength of the IDPs' 5.7-eV VEELS feature matches the 2175 Å astronomical feature, but the bandwidths are broader (Fig. 1). This extra breadth may result from the  $\sim 10$  times lower energy resolution of VEELS (relative to PAS) and from the grains' physical state. The subgrains within the IDPs are no longer free-floating in the ISM, and the extent of their solid-state modification during their  $\sim 4.5$ -billion-year post-ISM lifetimes is unknown. At the very least they may have undergone significant aggregation into larger (50- to 500-nm-diameter) grains, and computer-modeling best fits to the

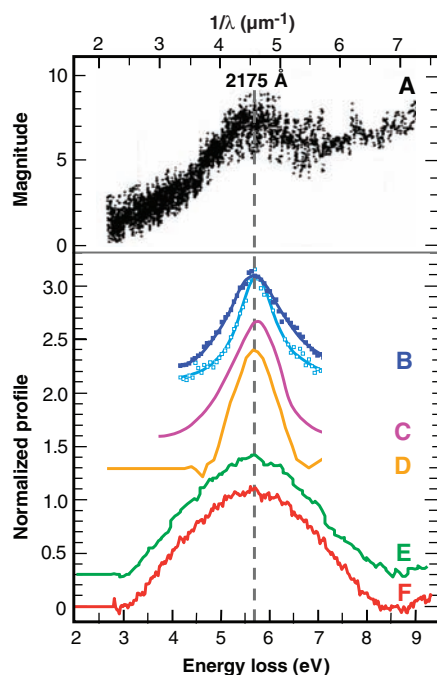


**Fig. 1.** Comparison of astronomical UV extinction features with laboratory UV and VEELS features. (A) The 2175 Å interstellar extinction feature from two stars  $\zeta$  and  $\epsilon$  Persei (5). (B) Broadest ( $\zeta$  Oph) and narrowest (HD 93028) profiles from 45 stars (6). (C) Photoabsorption spectrum from partially recrystallized amorphous magnesium silicate (8). (D) VEELS spectrum from (electron) irradiation-damaged talc ( $\text{Mg}_3\text{Si}_4\text{O}_{10}[\text{OH}]_2$ ). (E) VEELS spectrum from (organic) carbon in IDP L2047 D23. (F) VEELS spectrum from GEMS in W7013 E17.

astronomical 2175 Å feature are obtained with much smaller ( $<15$ -nm-diameter) grain sizes (1–4). Production of the interstellar 2175 Å feature is generally thought to be due to electronic transitions associated with the surfaces of small grains, and modification of these surfaces by aggregation, for example, is expected to alter the spectral profile of the feature (1, 22). Finally, all IDPs have been pulse heated to  $>350^\circ\text{C}$  during atmospheric entry (23) where organic components and  $-\text{OH}$ -bearing grains (e.g., GEMS) are particularly susceptible to modification.

IR spectroscopy of selected areas rich in carbonaceous material in our IDPs indicates that carbonyl (C=O) groups are the likely carrier of much of the oxygen in the organic fractions (Fig. 4). The average bulk carbon content of IDPs is  $\sim 12$  wt. % (21), at least half of which is hydrocarbons. About 10% of the carbon is bonded to oxygen, either in carbonyl (C=O) groups or as aromatic chromophores bound to hydroxyl ( $-\text{OH}$ ) groups (19, 21, 24). Multiple VEELS measurements sampling these regions show that the 5.7-eV feature strength correlates with the O/C ratio (Fig. 3, A to E). This suggests that the 5.7-eV feature produced by the carbonaceous subgrains in IDPs may be due to organic molecules (e.g., PAHs) with

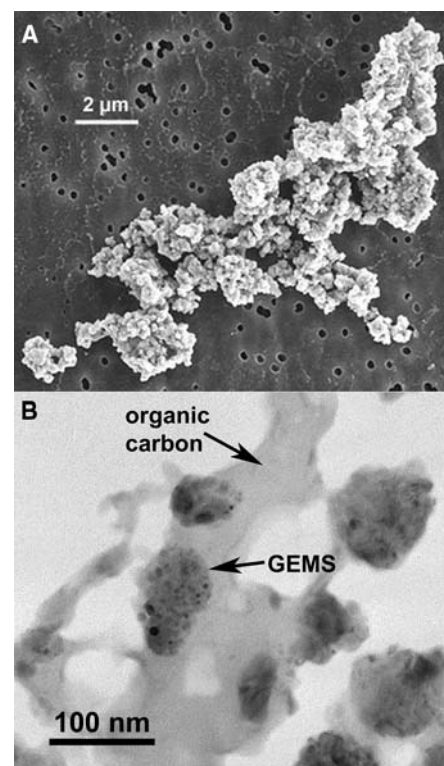


**Fig. 2.** (A) Secondary electron image of a typical chondritic IDP (RB12A). (B) A 200-keV brightfield transmission electron micrograph of organic carbon and GEMS within chondritic IDP L2009\*E2.

**Fig. 3.** VEELS spectra from subgrains in IDPs. (Left) Carbonaceous grains: (A) L2036-G16, ~500-nm-diameter grain, O/C = 0.41. (B) L2047 D23, ~800-nm-diameter grain with nonsolar  $^{14}\text{N}/^{15}\text{N}$  ratio of  $192 \pm 4$  ( $2\sigma$ ), O/C = 0.07. (C) L2036-C18-F4, ~400-nm-diameter grain with correlated nonsolar  $^{12}\text{C}/^{13}\text{C} = 80 \pm 2.4$  and  $^{14}\text{N}/^{15}\text{N} = 135 \pm 6.4$  isotopic compositions, O/C = 0.09. (D) Pyrene. (E) 1-Pyrene carboxaldehyde. (Right) GEMS: (F to H) W7013E17 (three GEMS, each 400 to 500 nm in diameter): (F)  $O_{\text{ex}} = 29.0$ , (G)  $O_{\text{ex}} = 19.1$ , (H)  $O_{\text{ex}} = 12.3$ . (I) L2036-C24-I3, ~650-nm-diameter grain, nonsolar  $^{16}\text{O}/^{17}\text{O} = 2262 \pm 108$ ,  $^{16}\text{O}/^{18}\text{O} = 403 \pm 8(9)$ ,  $O_{\text{ex}} = 2.3$ . (J) L2036-C18-F4, ~300-nm-diameter grain,  $O_{\text{ex}} = 1.6$ . Dashed lines indicate 5.7 eV. The weak 10.5-eV feature in GEMS spectra (right) is a silicate exciton [the position of which overlaps Lyman- $\alpha$  emission (5)].

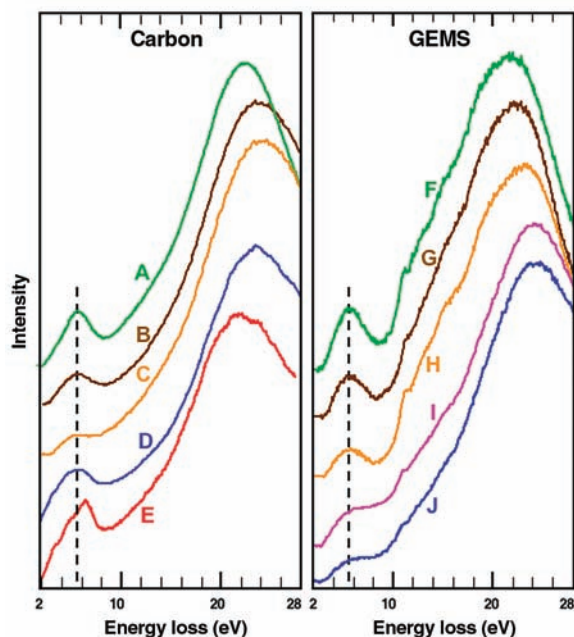
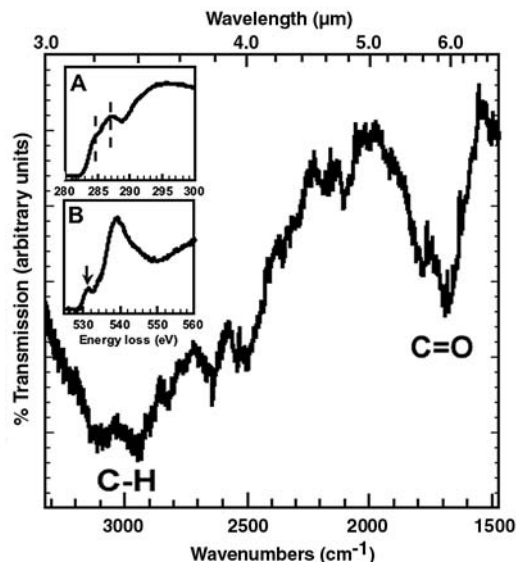


**Fig. 4.** IR spectrum from a ~9- $\mu\text{m}^2$  region of IDP L2036-G16 (Fig. 3A). Peaks at 2850 to 2960  $\text{cm}^{-1}$  are due to aliphatic C-H stretch modes, and the peak at ~1720  $\text{cm}^{-1}$  is due to carbonyl (C=O). Specimen thickness is <100 nm. (Insets) Electron energy-loss spectra recorded at 300 keV (no monochromator) of (A) carbon K-edge showing double  $\pi^*$  edges (dashed lines) at ~285.0 eV and 286.5 eV consistent with carbonyl (C=O), and (B) oxygen K-edge showing a pre-edge at ~531 eV (arrow) associated with a 1s to  $\pi^*$  transition of oxygen and also consistent with carbonyl (19, 21, 24).



carbonyl functionality. VEELS measurements of unsubstituted and carbonyl-substituted pyrene are consistent with this hypothesis (Figs. 3, D and E). Other measurements suggest that substituted PAHs are abundant in IDPs (24, 25), and laboratory simulations of radiation processing in dense clouds have demonstrated that carbonyl groups can be added to PAHs under some interstellar conditions (1, 26). Carbonyl-substituted PAHs are also present in carbonaceous chondrites (27).

Organic compounds may also be responsible for the 5.7-eV feature from GEMS because, in addition to being coated with carbon, some GEMS contain carbonaceous matter within their interiors (28). However, the strength of the GEMS 5.7-eV feature

correlates with increasing O concentration (Fig. 3, F to J), implicating the inorganic O-rich glassy matrices. Stoichiometric excesses of O ( $O_{\text{ex}}$ ) observed in GEMS may be due primarily to hydroxyl ions ( $\text{OH}^-$ ) within their amorphous magnesium silicate matrices (11). Laboratory UV spectra of hydroxylated amorphous magnesium silicate particles exhibit an absorption feature at 2175 Å that matches both the central wavelength and bandwidth of the interstellar feature (8) and may be due to an electronic transition of hydroxyl ions in low-coordination sites ( $\text{OH}^-_{\text{LC}}$ ) (Fig. 1C). In electron-irradiated talc ( $\text{Mg}_3\text{Si}_4\text{O}_{10}[\text{OH}]_2$ ) (Fig. 1D), the feature is also likely due to  $\text{OH}^-_{\text{LC}}$  because talc degrades (amorphizes) rapidly under the electron beam. Similarly, most of the hy-

droxyl in GEMS is probably  $\text{OH}^-_{\text{LC}}$  because the glassy matrices are defect-rich from constant irradiation in space (11).

Carbonaceous and amorphous silicate grains exhibiting a 5.7-eV (2175 Å) UV feature in VEELS spectra have been identified in chondritic IDPs collected in the stratosphere. The species implicated as possible carriers for these features are carbonyl-containing molecules and hydroxylated amorphous silicates (GEMS). However, because carbonaceous material permeates some GEMS, molecular matter may be solely responsible for the 5.7-eV feature. Both materials may have been produced by irradiation processing of dust in the ISM. Before this study, amorphous silicates, but not carbonyl compounds, were suggested as potential carriers of the astronomical 2175 Å extinction feature. On the basis of our observations of IDPs, we cannot conclude that organic carbon and (hydroxylated) amorphous silicates are the only carriers of the astronomical feature. However, the identification of interstellar subgrains in IDPs (as evidenced by their isotopic compositions) that produce analogous features suggests that the carrier(s) of the interstellar feature may be present in IDPs. This finding provides new information for computational modeling, laboratory synthesis of analog grains, and laboratory (UV) photo-absorption measurements. It is also worth looking for a correlation of the interstellar 2175 Å feature with IR carbonyl and hydroxyl bands, although lines-of-sight suitable for detecting a strong 2175 Å feature are generally diffuse, whereas larger column densities are typically required for detection of weaker infrared bands. The presence of two potential carriers may bear on the variable bandwidth of the astronomical feature, with relative abundance or physical state of each component varying from one sight line to another. Amorphous silicates are ubiquitous throughout interstellar space, but oxidized (carbonyl-containing) PAHs have yet to be identified in the ISM, although they are indicated as a major product of irradiation of PAHs and are found in primitive meteorites. A variety of exotic carriers for the 2175 Å peak have been proposed, including nanodiamonds, carbon onions, and fullerenes (1–4). However, organic carbon and amorphous silicates are more abundant in interstellar space, and cosmically abundant carriers are needed to explain the ubiquity of the 2175 Å feature.

#### References and Notes

- S. A. Sandford, *Meteorit. Planet. Sci.* **31**, 449 (1996).
- Th. Henning, F. Salama, *Science* **282**, 2204 (1998).
- B. T. Draine, *Annu. Rev. Astron. Astrophys.* **41**, 241 (2003).
- Th. Henning, C. Jäger, H. Mutschke, in *Astrophysics of Dust*, A. N. Witt, G. C. Clayton, B. T. Draine, Eds. [Astronomical Society of the Pacific (ASP) Conference Series, ASP, San Francisco, 2004], vol. 309, p. 603.

5. T. P. Stecher, *Astrophys. J.* **157**, L125 (1969).
6. E. L. Fitzpatrick, D. Massa, *Astrophys. J.* **307**, 286 (1986).
7. E. L. Fitzpatrick, D. Massa, *Astrophys. J. Suppl.* **72**, 163 (1990).
8. T. M. Steel, W. W. Duley, *Astrophys. J.* **315**, 337 (1987).
9. Collected IDPs are typically <20  $\mu\text{m}$  in diameter and are composed mostly of aggregated submicrometer grains including silicates, sulfides, metal, and inorganic and organic compounds (e.g., PAHs) (10). They are from comets and asteroids, they include the most chemically and isotopically primitive meteoritic materials available for laboratory investigations, and they are logical materials in which to look for carriers of the 2175  $\text{\AA}$  feature because they contain 10 to 100 times more interstellar material than the most primitive meteorites (11, 14).
10. J. P. Bradley, in *Treatise of Geochemistry*, A. M. Davis, H. D. Holland, K. K. Turekian, Eds. (Elsevier, Amsterdam, 2004), vol. 1, pp. 689–711.
11. J. P. Bradley, *Science* **265**, 925 (1994).
12. S. Messenger, L. P. Keller, F. Stadermann, R. M. Walker, E. Zinner, *Science* **300**, 105 (2003).
13. C. Floss, F. Stadermann, *Lunar Planet. Sci.* **XXXV**, abstr. 1281 (2004).
14. C. Floss *et al.*, *Science* **303**, 1355 (2004).
15. S. Messenger, *Nature* **404**, 968 (2000).
16. J. P. Bradley, Z. Dai, R. Erni, M. Browning, *Lunar Planet. Sci.* **XXXV**, abstr. 1433 (2004).
17. Materials and methods are available as supporting material on Science Online.
18. C. E. Brion, S. Daviel, R. Sodhi, A. P. Hitchcock, in *X-ray and Atomic Inner-Shell Physics—1982*, B. Crasemann, Ed. (American Institute of Physics Conference Proceedings No. 94, American Institute of Physics, New York, 1982), pp. 429–446.
19. G. J. Flynn, L. P. Keller, C. Jacobsen, S. Wirick, *Adv. Space Res.* **33**, 57 (2003).
20. S. A. Sandford *et al.*, *Astrophys. J.* **371**, 607 (1991).
21. L. P. Keller, S. Messenger, G. J. Flynn, S. Clemett, S. Wirick, C. Jacobsen, *Geochim. Cosmochim. Acta* **68**, 2577 (2004).
22. B. T. Draine, in *Interstellar Dust*, L. J. Allamandola, A. G. G. M. Tielens, Eds. (Kluwer, Dordrecht, Netherlands, 1989), pp. 313–327.
23. S. A. Sandford, J. P. Bradley, *Icarus* **82**, 146 (1989).
24. L. P. Keller, K. L. Thomas, D. S. McKay, in *Analysis of Interplanetary Dust*, M. E. Zolensky, T. L. Wilson, F. J. M. Rietmeijer, G. J. Flynn, Eds. (American Institute of Physics Conference Proceedings, American Institute of Physics, New York, 1994), vol. 310, pp. 51–87.
25. S. J. Clemett, C. R. Maechling, R. N. Zare, P. D. Swan, R. M. Walker, *Science* **262**, 721 (1993).
26. M. P. Bernstein *et al.*, *Astrophys. J.* **582**, L25 (2003).
27. J. R. Cronin, S. Chang, in *The Chemistry of Life's Origins*, J. M. Greenberg, C. X. Mendoza-Gomez, V. Pirronello, Eds. (Kluwer, Dordrecht, Netherlands, 1993), pp. 209–258.
28. D. E. Brownlee, D. J. Joswiak, J. P. Bradley, J. C. Gezo, H. G. M. Hill, *Lunar Planet. Sci.* **XXXI**, 1921 (2000).
29. This research was in part performed under the auspices of the U.S. Department of Energy (DOE), National Nuclear Security Administration, by the University of California under contract W-7405-Eng-48. The electron microscopy performed at the National Center for Electron Microscopy and infrared microspectroscopy performed at the Advanced Light Source (ALS) at Lawrence Berkeley National Laboratory are supported by the Director, Office of Science, Office of Basic Energy Sciences, Materials Sciences Division, DOE, under contract DE-AC03-76SF0098. This work was supported by NASA grants NAG5-10632 and NAG5-10696 (to J.B.) and grant NNG04GG49G (C.F.). We thank L. Nittler for image-processing software development and M. C. Martin and ALS personnel for beamline support. We also thank M. Bernas for performing the focused ion beam instrument work. We gratefully acknowledge discussions with M. Bernstein, D. Brownlee, B. Draine, Th. Henning, X. Tielens, and F. Salama.

## Supporting Online Material

www.sciencemag.org/cgi/content/full/307/5707/244/DC1

Materials and Methods

25 October 2004; accepted 10 December 2004  
10.1126/science.1106717

## Retinoic Acid Signaling Restricts the Cardiac Progenitor Pool

Brian R. Keegan,<sup>1</sup> Jessica L. Feldman,<sup>1</sup> Gerrit Begemann,<sup>2</sup>  
Philip W. Ingham,<sup>3</sup> Deborah Yelon<sup>1\*</sup>

Organogenesis begins with specification of a progenitor cell population, the size of which provides a foundation for the organ's final dimensions. Here, we present a new mechanism for regulating the number of progenitor cells by limiting their density within a competent region. We demonstrate that retinoic acid signaling restricts cardiac specification in the zebrafish embryo. Reduction of retinoic acid signaling causes formation of an excess of cardiomyocytes, via fate transformations that increase cardiac progenitor density within a multipotential zone. Thus, retinoic acid signaling creates a balance between cardiac and noncardiac identities, thereby refining the dimensions of the cardiac progenitor pool.

Generation of the proper number of organ progenitor cells is likely to involve interplay between inductive and repressive signaling pathways. Key inductive mechanisms have been identified for many organs, including the heart, but mechanisms for repressing progenitor fate assignment are poorly understood. Several factors, including Bmp2, Fgf8, Nodal, and Wnt11, are implicated in promoting the initial selection of myocardial progenitor cells from a multipotential popu-

lation (1). Although convergence of inductive signals might be sufficient to delimit the number of progenitor cells, opposing signals could also be necessary to restrict myocardial specification. Prior studies have suggested mechanisms for inhibiting cardiomyocyte differentiation within the anterior lateral plate mesoderm (ALPM), by means of Notch signaling (2) or interactions with the notochord (3), but little is known about whether repressive pathways limit the initial assignment of myocardial identity.

We find that reduction of retinoic acid (RA) signaling causes formation of an excess of cardiomyocytes. The zebrafish mutation *neckless* (*nls*) disrupts function of the *retinaldehyde dehydrogenase 2* gene (*raldh2*), which controls a rate-limiting step in RA synthesis (4, 5). *nls* mutants exhibit an increased number of cells expressing *nkx2.5*, a marker of the bilateral populations of precardiac mesoderm within the ALPM (Fig. 1A). Although *nkx2.5*

expression appears expanded in anterior, posterior, and lateral directions (Fig. 1, A and B), we do not observe an increase in the overall size of the ALPM in *nls* mutants (fig. S1A). As myocardial differentiation proceeds, *nls* mutants exhibit a surplus of cardiomyocytes, identifiable by their expression of *cardiac myosin light chain 2* (*cmlc2*) (Fig. 1B; fig. S1B). Formation of this myocardial surplus depends on the conventional myocardial differentiation pathway (1), which requires the activity of the growth factor Fgf8 and the transcription factors Hand2 and Gata5 (fig. S2). Consistent with a repressive influence of RA on cardiomyocyte formation, exposure to the pan-retinoic acid receptor (RAR) antagonist BMS189453 (6, 7) causes expansion of *nkx2.5* and *cmlc2* expression (Fig. 1, A and B). Conversely, exposure to exogenous RA results in a reduced number of cardiomyocytes (fig. S1C) (8). Together, these data demonstrate that cardiomyocyte population size within the ALPM is inversely related to the level of RA signaling.

The *raldh2* gene is expressed throughout early zebrafish embryogenesis (4, 5): In the blastula, *raldh2* is found at the embryonic margin; during gastrulation, *raldh2* is in involuting mesendoderm; and, after gastrulation, *raldh2* is in both lateral and paraxial mesoderm. To investigate when RA influences cardiomyocyte number, we tested the effectiveness of BMS189453 during different time intervals, initiating exposure at various stages and later assessing *nkx2.5* or *cmlc2* expression (Fig. 1, C and D; fig. S3). Addition of BMS189453 before gastrulation [40% epiboly, 5 hours post fertilization (hpf)] causes a myocardial expansion, whereas addition of BMS189453 during gastrulation (75% epiboly, 8 hpf) results in a more modest increase.

<sup>1</sup>Developmental Genetics Program, Skirball Institute of Biomolecular Medicine, and Department of Cell Biology, New York University School of Medicine, New York, NY 10016, USA. <sup>2</sup>Lehrstuhl Zoology/Evolutionary Biology, University of Konstanz, 78457 Konstanz, Germany. <sup>3</sup>Centre for Developmental Genetics, Department of Biomedical Science, University of Sheffield School of Medicine, Firth Court, Western Bank, Sheffield S10 2TN, UK.

\*To whom correspondence should be addressed.  
E-mail: yelon@saturn.med.nyu.edu